Growth, structure refinement, thermal expansion and optical spectroscopy of Tm3+-doped MgMoO4

Kirill Subbotin, Anatolii Titov, Denis Lis, Yulia Zimina, Yana Didenko, Ghassen Zin Elabedine, Kirill Eremeev, Rosa Maria Solé, Magdalena Aguiló, Pavel Volkov, et al.

Growth, structure and spectroscopy of Tm^{3+}-doped $MgMoO_4$

Kirill Subbotin[1,2], Anatolii Titov[1,2], Denis Lis[2], Yulia Zimina[1,2], Yana Didenko[1,2], Ghassen Zin Elabedine[3], Kirill Eremeev[4], Rosa Maria Solé[3], Magdalena Aguiló[3], Pavel Volkov[5], Pavel Popov[6], Elena Chernova[1], Francesc Díaz[3], Patrice Camy[4], Xavier Mateos[3,#] and Pavel Loiko[4,*]

[1]*Prokhorov General Physics Institute, Russian Academy of Sciences, 38 Vavilova St., 119991 Moscow, Russia*
[2]*Mendeleev University of Chemical Technology of Russia, 9 Miusskaya Sq. 125049 Moscow, Russia*
[3]*Universitat Rovira i Virgili (URV), Física i Cristal·lografia de Materials (FiCMA), Marcel·lí Domingo 1, 43007 Tarragona, Spain*
[4]*Centre de Recherche sur les Ions, les Matériaux et la Photonique (CIMAP), UMR 6252 CEA-CNRS-ENSICAEN, Université de Caen Normandie, 6 Boulevard Maréchal Juin, 14050 Caen Cedex 4, France*
[5]*NRC "Kurchatov Institute" — IREA Shared Knowledge Center, Moscow, Russia*
[6]*Petrovsky Bryansk State University, 14 Bezhitskaya St., 241023 Bryansk, Russia*
[#]*Serra Húnter Fellow*

**Corresponding author, e-mail: pavel.loiko@ensicaen.fr*

Abstract. Thulium-doped magnesium molybdate single-crystal (Tm^{3+}:$MgMoO_4$) was grown by the Czochralski method (melting point: 1322 °C). The actual Tm^{3+} doping level was measured to be 0.1 at.% (the segregation coefficient was only 0.02). Tm:$MgMoO_4$ belongs to the monoclinic class (sp. gr. *C*2/*m*, lattice constants: *a* = 10.2769(2) Å, *b* = 9.2898(5) Å, *c* = 7.0269(4) Å, *β* = 106.898(6)°). The thermal expansion tensor of this crystal is determined. Its thermal conductivity is also measured at 50 – 300 K (at room temperature, it amounts to 2.64 $Wm^{-1}K^{-1}$). Polarized Raman spectra are presented and the strongest mode is found at 957 cm^{-1}. Optical spectroscopy of Tm^{3+} ions is studied indicating broad emission bands extending beyond 2 μm (the $^3F_4 \rightarrow {}^3H_6$ transition) and a long lifetime of the $^3F_4$ excited-state (1.972 ms). This makes Tm:$MgMoO_4$ promising for broadly tunable and mode-locked lasers, when the technological problem of fabricating crystals with higher Tm^{3+} concentrations will be solved.

Keywords: molybdates; thulium ions; Czochralski method; crystal structure; Raman spectra; luminescence.

1. Introduction

Double tungstate and molybdate crystals containing the WO_4 / MoO_4 groups are attractive laser host media for doping with trivalent rare-earth ions (RE^{3+}) [1,2]. These crystals exhibit a great variety of structural types [3]. Among them, disordered tetragonal (sp. gr. $I4_1/a$) crystals $NaR(XO_4)_2$ [1] and ordered monoclinic (sp. gr. $C2/c$) crystals $KR(XO_4)_2$ [2] where R = Gd, Y, Lu and X = W / Mo are the most commonly used ones. In the past years, the crystal family of divalent metal monotungstates MWO_4 (where M = Mg, Zn, Mn, Cd, etc.), have attracted a lot of attention for RE^{3+} doping as well [4-6]. These crystals belong to the monoclinic class (sp. gr. $P2/c$) adopting the ordered wolframite-type structure [7,8].

One example: magnesium monotungstate crystal $MgWO_4$ which has been recognized as an excellent host for doping with various RE^{3+} ions such as Yb^{3+} [4,9], Er^{3+} [10], Tm^{3+} [5,11] or Ho^{3+} [12] owing to (i) good thermal and thermo-mechanical properties of the host matrix, (ii) strong natural birefringence, (iii) intense and strongly polarized spectral bands of the dopant RE^{3+} ions; (iv) strong crystal fields leading to large Stark splitting of the RE^{3+} multiplets and broad emission bands [13] and (v) Raman activity. The high thermal conductivity of $MgWO_4$ (8.7 $Wm^{-1}K^{-1}$ at room temperature [14]) makes it exceptional among other laser host crystals of the double tungstate / double molybdate families.

In particular, $MgWO_4$ crystals doped with thulium ions (Tm^{3+}) exhibit broadband strongly polarized emission extending beyond 2 μm (the $^3F_4 \rightarrow {}^3H_6$ transition) [13]. Recently, highly efficient, low threshold and wavelength-tunable lasing [11,13] was demonstrated using Tm:$MgWO_4$ crystals. Furthermore, the first generation of sub-100 fs pulses from a bulk solid-state laser at ~2 μm was demonstrated in 2017 using a Tm:$MgWO_4$ crystal [15]. Note that $MgWO_4$ crystals are grown by the Top-Seeded Solution Growth (TSSG) method (from the flux) [4,5].

The molybdate counterpart of $MgWO_4$ is also known, $MgMoO_4$ [16-18]. This crystal melts congruently and can be easily grown by the Czochralski (Cz) method. The structure of $MgMoO_4$ (Fig. 1) is different from that of $MgWO_4$, although it is also monoclinic. It belongs to the $C2/m$ space group and the $2/m$ point group, with the unit-cell parameters a = 10.273(3)Å, b = 9.288(3)Å, c = 7.025(2)Å and β = 106.96° [19]. The $MgMoO_4$ crystal shows a layered structure: the layers of two non-equivalent kinds of MgO_6 octahedra formed around Mg1 (Wyckoff: 4*g*) and Mg2 (Wyckoff: 4*i*) sites are separated by the layers of two non-equivalent kinds of MoO_4 tetrahedra. The neighbouring MgO_6 octahedra are connected by the shared edges. According to the structure refinement and EPR studies, the dopant RE^{3+} ions tend to replace for the host-forming cations Mg^{2+} in one of the lattice sites, namely, the Mg1 one [20,21]. This is because of the stronger distortion of the $Mg1O_6$ octahedra and longer Mg1 – O distances tolerating the difference in the ionic radii of VI-fold oxygen coordinated Mg^{2+} (0.72 Å) and, for example, Tm^{3+} (0.88 Å), as compared to almost ideal $Mg2O_6$ octahedrons with shorter metal – oxygen interatomic distances.

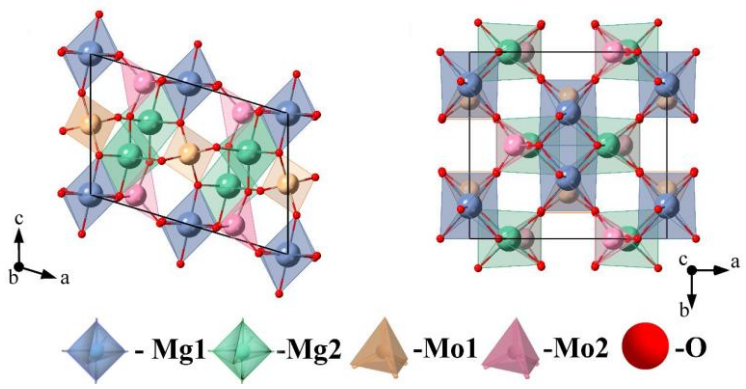

Figure 1. The structure of $MgMoO_4$ in two crystallographic projections (according to [22]), *black lines* – unit-cell.

The first successful attempts to grow $MgMoO_4$ single crystals by the Cz technique have been reported in 1963 [23], and in 1966 [24]. Later, the Cz technique has been successfully used for the growth of both undoped $MgMoO_4$ crystals [25-27], and crystals doped with Gd^{3+},Fe^{2+} [21], Yb^{3+} [25] and Nd^{3+} [28] ions. Cr^{3+} [16,18] and Yb^{3+} [29] doped $MgMoO_4$ single crystals have also been grown from $K_2Mo_2O_7$ [18,29] or $Na_2MoO_4 + MoO_3$ [16] fluxes, respectively.

The specific heat capacity and some other thermal properties of the $MgMoO_4$ crystal were measured in [18,30,31]. Various characteristics of flux-grown Cr^{3+}:$MgMoO_4$ single crystals have been studied [18], including linear thermal expansion coefficients and some mechanical strength characteristics (micro-hardness, crack resistance) along the three crystallographic directions.

The optical and spectroscopic properties of undoped $MgMoO_4$ fabricated by various techniques have been extensively studied to the moment [17,22,25,32-35]. Some data on spectroscopic properties are also available in the literature for $MgMoO_4$ crystals doped with Cr^{3+} [16,18], Yb^{3+} [25,29], Nd^{3+} [28], Eu^{3+} [36,37], Eu^{3+},Dy^{3+} [38], and Eu^{3+},Bi^{3+} ions [20]. Similar to most of the other molybdate crystals, undoped $MgMoO_4$ possesses its own broadband luminescence in the visible range under UV or X-ray excitation, as well as by electron beam or α-particles [17,22,25,32-35,37] due to the charge-transfer transition with the formation / recombination of self-trapped excitons at the $[MoO_4]$ clusters [12,25,34,39], moreover, luminescence due to deep traps at point defects or oxygen vacancies in the $[MoO_4]$ clusters [15,35]. Besides the luminescence decay, the excited-state energy can be easily transferred to the RE^{3+} dopants (e.g., Eu^{3+}, Yb^{3+}) with the subsequent luminescence through the above-mentioned centers [25,37]. Hence, this material is interesting for applications as scintillators [8,25], phosphors [11,33,37] and laser hosts [18]. Besides that, the $MgMoO_4$ powder is widely used as a catalyst for dehydrogenization of saturated hydrocarbons [40,41].

Meanwhile, no report on the growth nor studies of Tm^{3+}-doped $MgMoO_4$ crystals can be found in the literature. In the present work, we report on the successful Czochralski growth, as well as the structural, thermal and spectroscopic investigations of both undoped and Tm^{3+}-doped $MgMoO_4$ single crystals.

2. Experimental

2.1. Crystal growth

The single-crystals of $MgMoO_4$ and Tm:$MgMoO_4$ were grown by the Cz method at the “Kristall-2” growth machine (USSR) in air using a Pt/Rh crucible with a diameter / height of Φ30 mm / 30 mm, respectively, and a [001] oriented seed cut from an undoped $MgMoO_4$ single crystal. The raw materials were MgO (purity: 4N, Krasnyi Khimik, USSR), MoO_3 (4N, Lankhit Ltd., Russia), and Tm_2O_3 (4N, USSR). The Tm^{3+} content in the initial melt for the growth of Tm:$MgMoO_4$ was 5 at.% with respect to Mg^{2+} ions. No charge compensators were used.

Prior to melting, the blend of the initial chemicals was thoroughly mixed and calcined at 700 °C during 5 hours (h) for solid-phase synthesis. Without calcining, a substantial part of MoO_3 would evaporate from the melt as the saturated vapor pressure of unbound MoO_3 at the $MgMoO_4$ melting point (1322 °C, see below) exceeds 1 atm.

The pulling rate / rotation speed were 1 mm/h and 6 revolutions per minute (rpm), respectively. When the growth was completed, the crystals were slowly cooled down to

room temperature (RT, 20 °C) at a rate of 8 °C/h to reduce the risk of crystal cracking. Then, the crystals were additionally annealed in air at 800 °C for 2 weeks.

2.2. Characterization methods

The actual Tm^{3+} concentration in the $MgMoO_4$ crystal was measured by inductively coupled plasma atomic emission spectroscopy (ICP–AES) using an iCAP6300 duo Thermo Fisher Scientific spectrometer. Before the measurement, a piece of the crystal was thoroughly ground into powder and dissolved in H_3PO_4 (Suprapur, Merck) at a temperature of 400 °C.

Another piece of the as-grown crystal was ground into powder for X-ray powder diffraction (XRD) analysis. These measurements were carried out using a Bruker-AXS D8-Advance diffractometer with a vertical θ-θ goniometer and Cu Kα radiation. The detection of the diffracted X-rays was made with a LynxEye-XE-T PSD detector with an opening angle of 2.94°. The data were collected in the 2θ interval from 5 to 90°, with step size of 0.02° and step time of 2 s. The measured XRD pattern was refined by the Rietveld method using the Topas V6 software. The crystal structure of undoped $MgMoO_4$ (PDF #72-2153, ICSD database) [19] was used as the initial model for the Rietveld refinement. XRD measurements at elevated temperatures, from RT to 650 °C, were performed to calculate the linear thermal expansion coefficients. The same diffractometer was used with the same step size / time, and the measurements were made in the 2θ range from 5 to 80°. A delay of 300 s was applied before each measurement. The crystal to be used for optical characterization was oriented in the crystallographic frame using single-crystal X-ray diffraction.

The differential thermal analysis (DTA) from RT to 1400 °C, in heating and cooling processes, was performed using a TA Instruments SDT 2960 equipment. The measurements were carried out in Pt crucibles and Al_2O_3 was used as a reference material. The heating and cooling rates were 10 °C/min, under a nitrogen flow of 140 cm^3/min.

The thermal conductivity of undoped $MgMoO_4$ was measured by the method of stationary longitudinal heat flow in the temperature range of 50 – 300 K using an [001]-oriented crystal. To ensure a plane shape of the isothermal surfaces, the resistive heater was glued to the end surface of the sample. The measurement error did not exceed ±6 %. More details can be found elsewhere [42].

The polarized Raman spectra were measured for a [010]-cut crystal using a confocal laser microscope (InVia, Renishaw) equipped with a ×50 Leica objective and an Ar^+ ion laser (514 nm). The unpolarized absorption spectra were measured using a Varian Cary 5000 spectrophotometer. The polarized luminescence spectra were measured using a Glan-Taylor polarizer and an optical spectrum analyzer (AQ6376, Yokogawa) with a ZrF_4 fiber. The luminescence decay was studied using a ns optical parametric oscillator (Horizon, Continuum), a 1/4 m monochomator (Oriel 77200), an InGaAs detector and an 8 GHz digital oscilloscope (DSA70804B, Tektronix).

3. Results and discussion

3.1. Grown crystals

The photographs of the as-grown $MgMoO_4$ and Tm:$MgMoO_4$ crystals are shown in Fig. 2. Both crystals exhibited a bright saffron-yellow coloration, with a maximum diameter of ~15-16 mm and a length of ~40-50 mm. The boules demonstrated a highly expressed natural faceting. Besides that, the Tm:$MgMoO_4$ crystal contained a couple of cleavage cracks. Spasskii *et al.* identified one of the cleavage planes of $MgMoO_4$ as {9 11 0} [25]. The cracks were flat and nearly perpendicular to each other confirming the identification of the cleavage planes proposed in [25].

Figure 2. Photographs of the as-grown crystal boules of (a) undoped $MgMoO_4$ and (b) 0.1 at.% Tm^{3+}-doped $MgMoO_4$ (actual doping level). The growth direction is along the [001] axis.

During the growth of magnesium molybdate crystals, a pronounced volatility of MoO_3 from the surface of the melt was observed. The vapor then condensated at cold elements of the growth zone (i.e., the heat insulating ceramics, the upper parts of the seed holder) as needle-shaped yellow crystallites. Such volatility has been discussed previously [18,29] and it can result in the formation of molybdenum vacancies in the grown crystals. On the other hand, the usage of a single-crystalline $MgMoO_4$ seed under such circumstances may be considered as if it experiences annealing in MoO_3 vapor atmosphere. We have observed that after the usage of a $MgMoO_4$ seed in several crystal growth processes, its coloration step-by-step changed from saffron-yellow to pale yellowish, almost colorless one. This motivated us to study the absorption of such samples.

Figure 3 shows the absorption spectra of an undoped $MgMoO_4$ crystal before and after its usage as a seed for further molybdate crystal growth. The as-grown crystal exhibits rather strong and broad absorption band centered at ~430 nm, which causes the saffron-yellow coloration. After the usage as a seed (annealing in MoO_3 vapor atmosphere), the intensity of this absorption band drastically decreased, although, it did not disappear completely. This indicates that the concentration of the corresponding vibronic color centers in the crystal was substantially reduced after such an annealing. Note that annealing of the same crystal in air does not lead to the same effect indicating that the observed color centers are related with molybdenum deficiency.

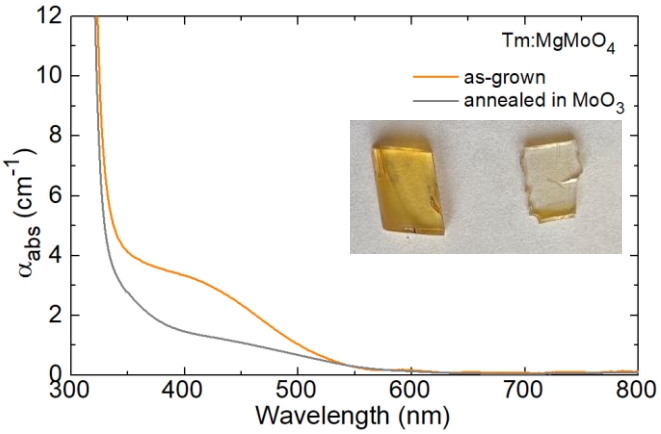

Figure 3. Unpolarized absorption spectra of the as-grown $MgMoO_4$ crystal, and a seed cut from this crystal after its annealing in the MoO_3 vapor atmosphere, *inset* – photograph of the polished crystal plates.

The coloration of scheelite-type double molybdate crystals was analyzed previously [43], including the saffron-yellow one which appeared sometimes in such crystals after their annealing in air. It was concluded that such coloration is caused by a hole center at the molybdenum vacancy. It seems that similar color centers are also formed in the $MgMoO_4$ crystals, while the annealing in MoO_3 vapor atmosphere eliminates them.

The actual Tm^{3+} concentration in the Tm:$MgMoO_4$ crystal was measured to be 0.1 at.% with respect to Mg^{2+} corresponding to an ion density $N_{Tm} = 0.13\times10^{20}$ cm^{-3}. According to the ratio between the actual dopant concentration in the crystal and its nominal concentration in the initial melt, the Tm^{3+} segregation coefficient was determined, K_{Tm} = 0.02. Previosuly, the segregation coefficient of Nd^{3+} in $MgMoO_4$ was also determined to be rather low, $K_{Nd} < 0.01$ [28].

Such a low value is typical for RE^{3+} dopant ions in Mg^{2+}-containing crystals. For example, the Yb^{3+} segregation coefficient between the Mg_2SiO_4 crystal and the melt is as low as 0.0009 [44]. It is due to the heterovalent character of the $Mg^{2+} \rightarrow Tm^{3+}$ substitution, as well as the essential difference in the ionic radii of these cations, namely 0.72 Å (Mg^{2+}) and 0.88 Å (Tm^{3+}) for VI-fold oxygen coordination. We believe that the choice of a proper charge compensator may substantially increase the segregation coefficient of Tm^{3+} ions in $MgMoO_4$. Indeed, according to the previous studies, the usage of a proper amount of Li^+ charge compensator doubles the Yb^{3+} segregation coefficient in Yb^{3+},Li^+:$ZnWO_4$ crystals as compared to singly Yb^{3+}-doped ones [45], whereas the usage of Nb^{5+} charge compensator raises the Nd^{3+} segregation coefficient in Nd^{3+},Li^+:$CaMoO_4$ by an order of magnitude (up to almost unity) in comparison with solely Nd^{3+}-doped $CaMoO_4$ crystals [46].

3.2. Crystal structure

Two polymorphs of $MgMoO_4$ are known. The α-phase possesses a cuproscheelite-type structure (sp. gr. *P*-1), similar to CuMoO4 and α-$ZnMoO_4$ [47]. The β-phase adopts the monoclinic structure (sp. gr. *C*2/*m*) and it is isostructural to the high-temperature phase of α-$MnMoO_4$ [48].

Figure 4 shows the measured X-ray powder diffraction pattern of the as-grown 0.1 at.% Tm:$MgMoO_4$ crystal together with the results of the Rietveld refinement. Tm:$MgMoO_4$ belongs to the monoclinic class (β-phase, sp. gr. C^3_{2h} - *C*2/*m*, No. 12, point group 2/*m*) and it is isostructural to undoped β-$MgMoO_4$. The inspection of the XRD pattern reveals no other phases except the monoclinic one. The refined lattice constants are a = 10.2769(2) Å, b = 9.2898(5) Å, c = 7.0269(4) Å and $\beta = \boldsymbol{a}\hat{}\boldsymbol{c}$ = 106.898(6)° (the number of formula units in the unit-cell: Z = 8), the volume of the unit-cell V = 641.902(7) $Å^3$ and the calculated crystal density ρ_{calc} of 3.888 g/cm^3. The determined lattice parameters are slightly larger than those for undoped β-$MgMoO_4$ powders reported in [19,39]. The calculated pattern well matched the experimental one and the refinement converged as indicated by the reliability factors, R_p = 4.93%, R_{wp} = 8.10% and R_{exp} = 2.61% (the reduced chi-squared: $\chi^2 = (R_{wp}/R_{exp})^2 = 9.61$). The fractional atomic coordinates, site occupancy factors and isotropic displacement parameters attained in the Rietveld refinement are listed in Table 1.

The metal – to – oxygen (Mg – O and Mo – O) interatomic distances are listed in Table 2. The corresponding polyhedra [$Mg1O_6$], [$Mg2O_6$], [$Mo1O_4$] and [$Mo2O_4$] are drawn in Fig. 5.

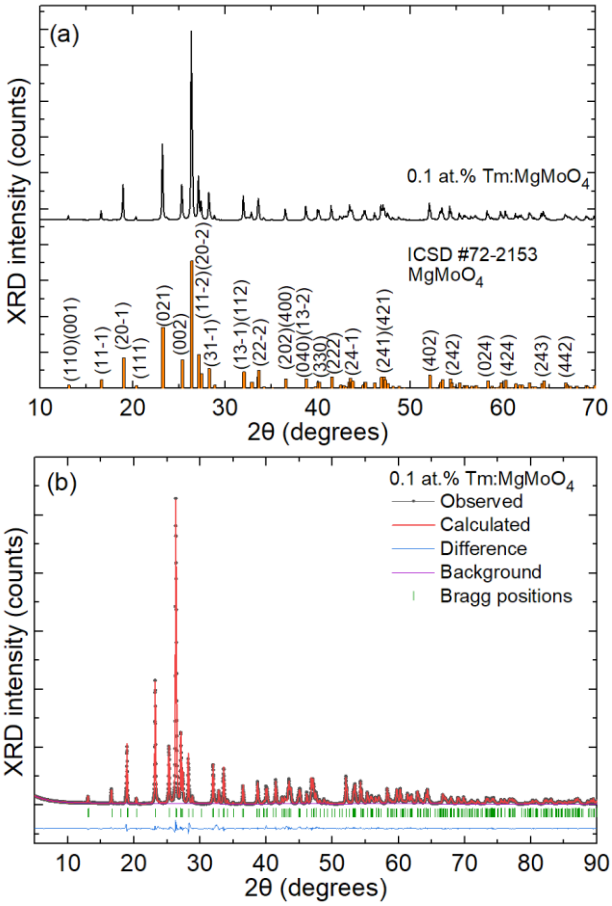

Figure 4. X-ray powder diffraction (XRD) study of the 0.1 at.% Tm:$MgMoO_4$ crystal: (a) measured XRD pattern, the theoretical pattern for $MgMoO_4$ (ICSD card No. 72-2153 is shown for comparison), *numbers* – Miller's indices, (*hkl*); (b) Rietveld refinement plots: measured, calculated, and residual profiles, *vertical dashes* – Bragg reflections.

Table 1. Fractional atomic coordinates (*x*/*a*, *y*/*b*, *z*/*c*), site occupancy factors (O.F.) and isotropic displacement parameters (B_{iso}) for 0.1 at.% Tm:$MgMoO_4$.

Atoms	*x*/*a*	*y*/*b*	*z*/*c*	O.F.	B_{iso}, Å^2	Wyckoff	Symmetry
Mg1	1/2	0.1791(3)	0	0.999	1.661(9)	4*g*	2
Tm	1/2	0.1791(3)	0	0.001	1.661(9)	4*g*	2
Mg2	0.7981(3)	1/2	0.6398(5)	1	0.056(7)	4*i*	*m*
Mo1	1/2	0.2523	1/2	1	0.105(6)	4*h*	2
Mo2	0.5433(2)	1/2	0.0955	1	0.068(4)	4*i*	*m*
O1	0.2121(3)	0.1505(9)	0.3088(9)	1	0.658(3)	8*j*	1
O2	0.3603(3)	0.3598(4)	0.3765(4)	1	1.182(3)	8*j*	1
O3	0.8552(6)	1/2	0.9577(8)	1	0.862(2)	4*i*	*m*
O4	0.6351(1)	0.3437(7)	0.0301	1	0.063(7)	8*j*	1
O5	0.2963(1)	0	0.3558(2)	1	0.294(7)	4*i*	*m*

Table 2. Selected interatomic (metal – oxygen) distances for 0.1 at.% Tm:$MgMoO_4$.

[$Mg1O_6$]	Å	[$Mg2O_6$]	Å	[$Mo1O_4$]	Å	[$Mo2O_4$]	Å
Mg1-O1	2.066	Mg2-O1	2.126	Mo1-O1	1.807	Mo2-O3	1.845
Mg1-O1	2.066	Mg2-O1	2.126	Mo1-O1	1.807	Mo2-O4	1.730

Mg1-O3	2.172	Mg2-O2	2.055	Mo1-O2	1.724	Mo2-O4	1.730
Mg1-O3	2.172	Mg2-O2	2.055	Mo1-O2	1.724	Mo2-O5	1.752
Mg1-O4	2.033	Mg2-O3	2.158				
Mg1-O4	2.033	Mg2-O5	2.001				

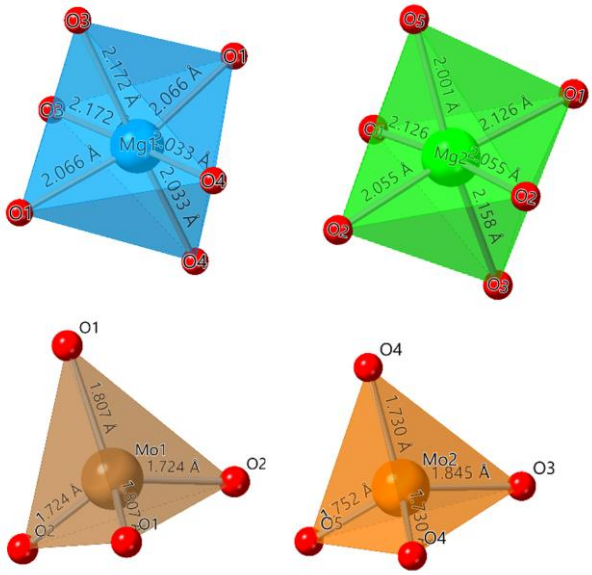

Figure 5. [$Mg1O_6$], [$Mg2O_6$], [$Mo1O_4$] and [$Mo2O_4$] polyhedra for the 0.1 at.% Tm:$MgMoO_4$ crystal.

3.3. DTA analysis

The DTA analysis of the Tm:$MgMoO_4$ crystal performed in the temperature range of 20-1400 °C revealed only one sharp thermal effect at 1322 °C corresponding to congruent melting / crystallization, see Fig. 6. This value nearly coincides with that reported in [49] for undoped $MgMoO_4$, 1320 °C.

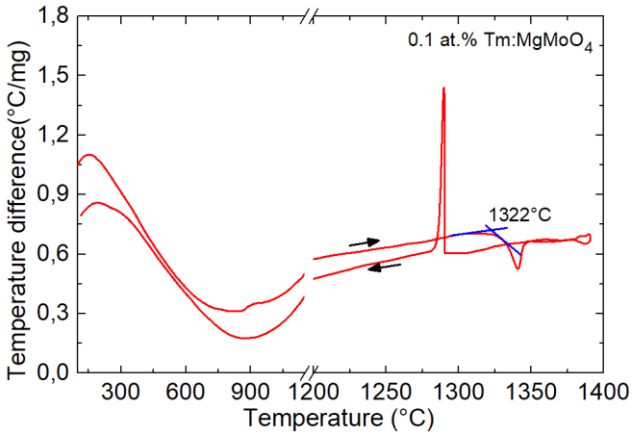

Figure 6. Differential thermal analysis (DTA) curve for the 0.1 at.% Tm:$MgMoO_4$ crystal.

3.4. Thermal expansion

According to the results of the performed high-temperature XRD analysis of the Tm:$MgMoO_4$ crystal, Fig. 7, the linear thermal expansion tensor α_{ij} has been constructed in the crystallo-physical frame {X_1, X_2, X_3}, where X_1 || ***a***, X_2 || ***b*** and X_3 || ***c****, where ***c**** is the axis orthogonal to the ***a***-axis and lying in the ***a***-***c*** plane:

$$(a_{ij}) = \begin{pmatrix} 7.089 & 0 & 0.222 \\ 0 & 14.30 & 0 \\ 0.222 & 0 & 3.706 \end{pmatrix} \times 10^{-6}\ \mathrm{K}^{-1}. \quad (1)$$

The tensor was then diagonalized to find the eigen-frame of thermal expansion {X_1', X_2', X_3'} and the corresponding diagonal tensor elements. The eigen-frame orientation is: the X_1' axis is rotated at an angle of 3.74° from the ***a*** axis clockwise, the X_2' axis is parallel to the ***b*** axis and the X_3' axis is rotated at an angle of 13.16° from the ***c*** axis (anticlockwise), with the ***b*** axis pointing towards the observer. In this coordinate system, the linear thermal expansion tensor of Tm:$MgMoO_4$ is:

$$(a'_{ij}) = \begin{pmatrix} 7.103 & 0 & 0 \\ 0 & 14.30 & 0 \\ 0 & 0 & 3.691 \end{pmatrix} \times 10^{-6}\ \mathrm{K}^{-1}. \quad (2)$$

Our results reasonably agree with the previous report on the linear thermal expansion coefficients of a Cr:$MgMoO_4$ crystal measured by the dilatometry method along the three crystallographic axes: $\alpha_a = 10.10\times10^{-6}\ K^{-1}$, $\alpha_b = 12.26\times10^{-6}\ K^{-1}$ and $\alpha_c = 3.71\times10^{-6}\ K^{-1}$ [18].

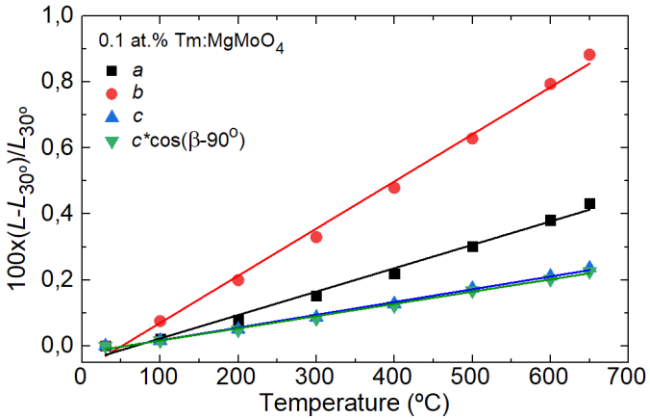

Figure 7. Evolution of the lattice parameters of 0.1 at.% Tm:$MgWO_4$ with temperature.

3.5. Thermal conductivity

The thermal conductivity κ of the undoped $MgMoO_4$ crystal was measured along the [001] direction in the temperature range of 50 – 300 K. It monotonously decreases with temperature, from 19.51 to 2.64 $Wm^{-1}K^{-1}$, as shown in Fig. 8. A similar behavior has been observed recently for $ZnWO_4$ and $CdWO_4$ crystals [50]. The thermal conductivity of $MgMoO_4$ at 300 K is only slightly lower than that of $ZnWO_4$ (κ = 3.2 $Wm^{-1}K^{-1}$ along the [010] direction [50]) and is greatly reduced as compared to that of $MgWO_4$ (κ = 8.7 $Wm^{-1}K^{-1}$ along arbitrary direction [14]).

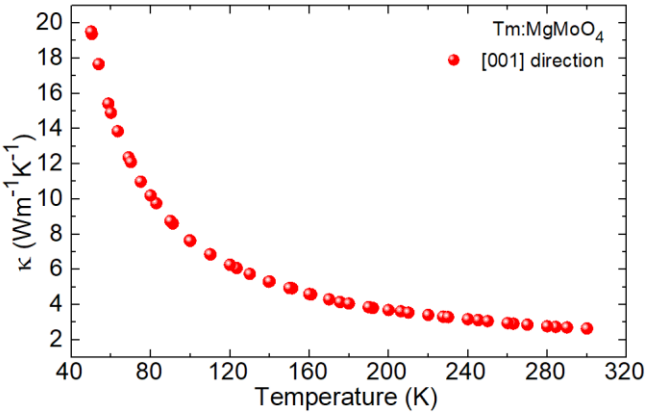

Figure 8. Thermal conductivity of undoped $MgMoO_4$ along the [001] direction as a function of temperature.

3.6. Raman spectra

For the monoclinic β-phase of $MgMoO_4$, there are 8 molecules per unit cell. The group theory analysis predicts the following set of irreducible representations of the factor group C_{2h} in the center of the Brillouin zone (***k*** = 0): $\Gamma = 19A_g + 17B_g + 14A_u + 19B_u$ (optical modes) [48, 51]. The even (*gerade*) modes (A_g and B_g) are Raman-active and uneven (*ungerade*) one (A_u and B_u) are IR-active. Among the Raman-active modes, 18 modes ($11A_g + 7B_g$) are the internal ones of the $[MoO_4]^{2-}$ tetrahedral: symmetric stretching (ν_1, $2A_g$), anti-symmetric stretching (ν_3, $3A_g + 3B_g$), symmetric bending (ν_2, $3A_g + 1B_g$), and anti-symmetric stretching (ν_4, $3A_g + 3B_g$).

The polarized Raman spectra of a ***b***-cut Tm:$MgMoO_4$ crystal are shown in Fig. 9. Here, Porto's notations are used. The Raman spectra contain intense peaks within two distinct ranges, 122 – 424 cm^{-1} and 754 – 969 cm^{-1}, which is a typical behavior for monoclinic tungstate / molybdate crystals. The peaks from the low-frequency band are due to the lattice vibrations and some bending modes (ν_2 and ν_4) mixed with the lattice vibrations. The peaks from the high-frequency band are due to the stretching (ν_1 and ν_3) vibrations of the $MgMoO_4$ tetrahedra. The most intense mode appears at 957 cm^{-1} and the highest phonon energy is 969 cm^{-1}. Both these peaks are due to symmetric stretching (ν_1, $2A_g$) vibrations. Their peak linewidths (FWHM) are ~6 cm^{-1}.

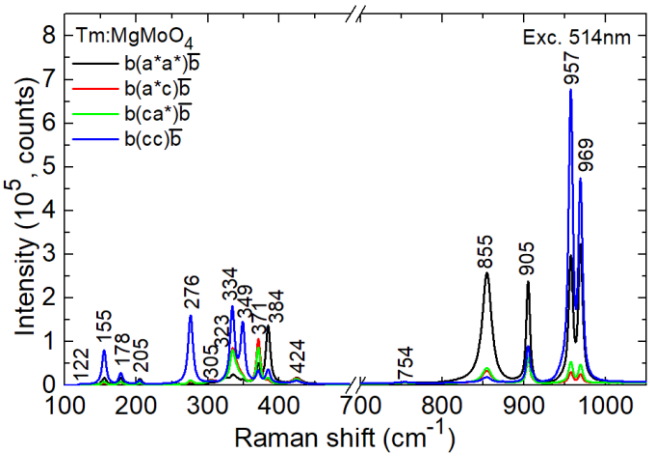

Figure 9. Polarized Raman spectra of a [010]-cut 0.1 at.% Tm:$MgMoO_4$ crystal, λ_{exc} = 514 nm, *numbers* – Raman frequencies in cm^{-1}.

3.7. Optical spectroscopy of Tm^{3+} ions

Due to the weak absorption of Tm^{3+} ions in a low-doped Tm:$MgMoO_4$ crystal, only the unpolarized optical absorption spectrum of the as-grown crystal was measured, Fig. 10. Here, the absorption bands are due to transitions of Tm^{3+} ions from the ground-state ($^3H_6$) to the excited-states $^3F_4$ (~1.63 μm), $^3H_5$ (~1.21 μm), $^3H_4$ (~0.79 μm) and $^3F_{2,3}$ (~0.68 μm). The broad absorption bands in the visible and near-IR underlying the Tm^{3+} bands are due to the above-mentioned color centers. For the $^3H_6 \rightarrow {}^3H_4$ Tm^{3+} transition which is usually used for optical pumping, e.g., by commercial AlGaAs laser diodes, the estimated peak absorption cross-section σ_{abs} is 1.60×10^{-20} cm^2 at 794.2 nm corresponding to an absorption bandwidth (full width at half maximum, FWHM) of 6.6 nm. This value is broader than that for scheelite-type molybdates, e.g., ~5 nm for Tm:$NaLa(MoO_4)_2$ [52].

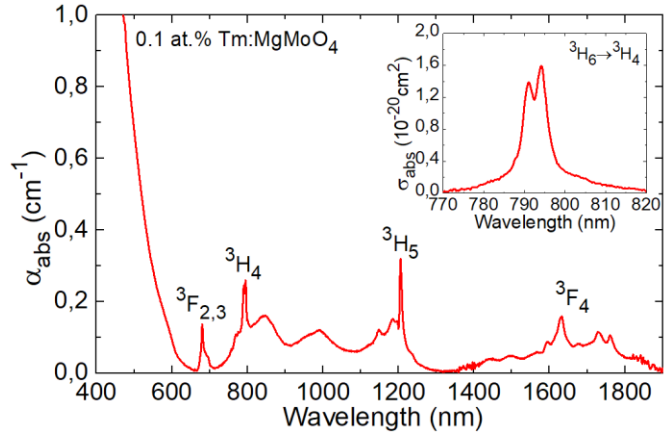

Figure 10. Unpolarized absorption spectrum of the 0.1 at.% Tm:$MgMoO_4$ crystal, *inset* – absorption band corresponding to the $^3H_6 \rightarrow {}^3H_4$ Tm^{3+} transition.

Tm^{3+} ions in $MgMoO_4$ exhibit a broad and smooth emission band spanning from 1.6 up to 2.15 μm related to the $^3F_4 \rightarrow {}^3H_6$ transition, Fig. 11. The luminescence spectra are strongly polarized, with the highest emission intensity for light polarization ***E*** || ***a****. They extend well beyond 2 μm (e.g., the long-wave emission peaks at which laser operation is expected are found at ~2000 nm and ~2050 nm) thus avoiding the structured water vapor absorption in air. This feature makes Tm:$MgMoO_4$ promising for generation of ultrashort (fs) pulses from mode-locked lasers.

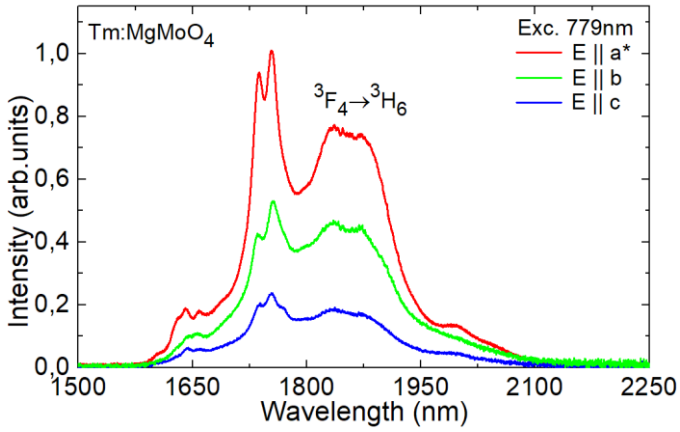

Figure 11. Polarized luminescence spectra of Tm^{3+} ions in $MgMoO_4$ (the $^3F_4 \rightarrow {}^3H_6$ transition), λ_{exc} = 779 nm.

The luminescence decay curve from the $^3F_4$ state of Tm^{3+} ions in $MgMoO_4$ is nearly single-exponential, see Fig. 12. It indicates that Tm^{3+} ions are located mostly in one of the two non-equivalent Mg^{2+} sites of the structure, in agreement with the conclusion made previously based on EPR studies for other RE^{3+} ions [20,21]. Another possibility is that for both sites, the Tm^{3+} ions show close transition probabilities. The measured luminescence lifetime of the $^3F_4$ excited state τ_{lum} is relatively long, 1.972 ms and it is close to that for Tm:$MgWO_4$ (τ_{lum} = 1.93 ms) [11] and essentially longer than that for Tm^{3+} ions in scheelite-type molybdates (τ_{lum} = 1.1 ms for $NaLa(MoO_4)_2$ [52]). A long lifetime of the upper laser level is favorable for low-threshold laser generation.

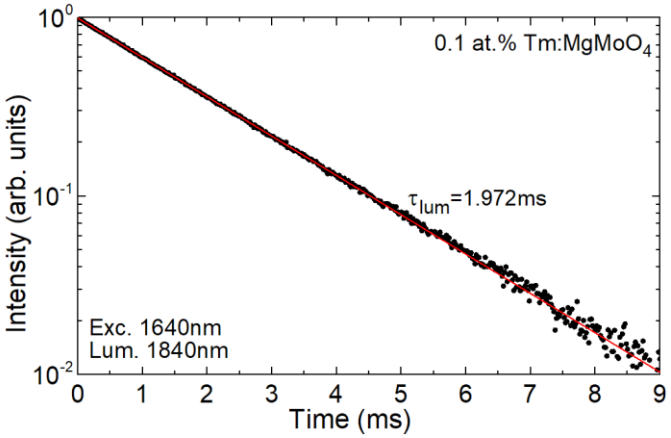

Figure 12. Luminescence decay curve from the $^3F_4$ state of Tm^{3+} ions in the $MgMoO_4$ crystal, λ_{exc} = 1640 nm, λ_{lum} = 1840 nm, *red line* – single-exponential fit.

4. Conclusions

To conclude, we report on the Czochralski growth, Rietveld structure refinement, thermal, vibronic and spectroscopic properties of a thulium-doped magnesium molybdate, Tm^{3+}:$MgMoO_4$, belonging to the crystal family of monoclinic divalent metal mono-tungstates / molybdates, which are currently attracting a lot of attention as laser gain media suitable for high-power / ultrashort-pulse generation. Disordered Tm^{3+}:$MgMoO_4$ adopts a monoclinic structure (sp. gr. *C*2/*m*) being different from that of the ordered Tm:$MgWO_4$ crystal (sp. gr. *P*2/*c*) and featuring two non-equivalent sites for the host-forming Mg^{2+} cations (still, it seems the dopant Tm^{3+} ions predominantly reside in only one type of sites). The difference in the ionic radii and the valence state of Mg^{2+} and Tm^{3+} probably determine the low segregation coefficient of the latter which is expected to be improved when introducing proper charge compensators. Still, the Cz growth attempt was successful for Tm^{3+}:$MgMoO_4$ resulting in large-volume transparent crystals with a bright yellow coloration. It seems to be associated with hole centers at molybdenum vacancies and can be eliminated to a great extent by annealing in MoO_3 vapor atmosphere. The thermal conductivity of Tm^{3+}:$MgMoO_4$ at room temperature is moderate (2.64 $Wm^{-1}K^{-1}$) still being much higher than that of disordered tetragonal sodium rare-earth double molybdates.

In terms of spectroscopic properties, Tm^{3+} ions in $MgMoO_4$ feature (i) broad absorption around 0.8 μm, (ii) smooth and broad emission bands owing to the $^3F_4 \rightarrow {}^3H_6$ transition extending well above 2 μm thus making this crystal attractive for ultrashort pulse generation, (iii) strongly polarized emission spectra which is a prerequisite for linearly polarized laser emission, (iv) long luminescence lifetime of the $^3F_4$ state and (v) intense and strongly polarized Raman spectra. For achieving laser operation, crystals with higher Tm^{3+} doping levels are necessary.

Acknowledgments

The research was supported by the Ministry of Science and Higher Education of Russia (project No. FSSM-2020-0005). The ICP-AES analysis was done using equipment of the NRC “Kurchatov Institute” — IREA Shared Knowledge Center under financial support by the Russian Federation, represented by the Ministry of Science and Higher Education, agreement No. 075-15-2022-1157 dd. 16.08.2022. Grant PID2019-108543RB-I00 funded by MCIN/AEI/10.13039/501100011033. Grant PECT “Cuidem el que ens uneix", operation 4 Sensòrica, Act 4 Fotònica” PR15-020174 co-financed by the European Regional

Development Fund “ERDF A way of making Europe” through the ERDF Catalonia Operational Programme 2014-2020.

References

1. J. M. Cano-Torres, M. Rico, X. Han, M. D. Serrano, C. Cascales, C. Zaldo, V. Petrov, U. Griebner, X. Mateos, P. Koopmann, C. Kränkel, Comparative study of crystallographic, spectroscopic, and laser properties of Tm^{3+} in $NaT(WO_4)_2$ (T = La, Gd, Y, and Lu) disordered single crystals, Phys. Rev. B 84 (2011) 174207-1–15.
2. V. Petrov, M. C. Pujol, X. Mateos, Ò. Silvestre, S. Rivier, M. Aguiló, R. M. Solé, J. H. Liu, U. Griebner, and F. Díaz, Growth and properties of $KLu(WO_4)_2$, and novel ytterbium and thulium lasers based on this monoclinic crystalline host, Laser Photon. Rev. 1 (2007) 179-212.
3. P.V. Klevtsov, R.F. Klevtsova, Polymorphism of the double molybdates and tungstates of mono- and trivalent metals with the composition $M^+R^{3+}(EO_4)_2$, J. Struct. Chem. 18 (1977) 339-355.
4. L. Zhang, W. Chen, J. Lu, H. Lin, L. Li, G. Wang, G. Zhang, and Z. Lin, Characterization of growth, optical properties, and laser performance of monoclinic Yb:$MgWO_4$ crystal, Opt. Mater. Express 6 (2016), 1627-1634.
5. L. Zhang, H. Lin, G. Zhang, X. Mateos, J. M. Serres, M. Aguiló, F. Díaz, U. Griebner, V. Petrov, Y. Wang, P. Loiko, E. Vilejshikova, K. Yumashev, Z. Lin, and W. Chen, Crystal growth, optical spectroscopy and laser action of Tm^{3+}-doped monoclinic magnesium tungstate, Opt. Express 2 (2017), 3682-3693.
6. A. Volokitina, S.P. David, P. Loiko, K. Subbotin, A. Titov, D. Lis, R.M. Solé, V. Jambunathan, A. Lucianetti, T. Mocek, P. Camy, U. Griebner, V. Petrov, M. Aguiló, F. Díaz, and X. Mateos, Monoclinic zinc monotungstate Yb^{3+},Li^+:$ZnWO_4$: Part II. Polarized spectrosocpy and laser operation, J. Lumin. 231 (2021) 117811-1-12.
7. V.B. Kravchenko, Crystal structure of the monoclinic form of magnesium tungstate $MgWO_4$, J. Struct. Chem. 10 (1969) 139-140.
8. V.B. Mikhailik, H. Kraus, V. Kapustyanyk, M. Panasyuk, P. Yu, V. Tsybulskyi, and L. Vasylechko, Structure, luminescence and scintillation properties of the $MgWO_4$ – $MgMoO_4$ system, J. Phys.: Cond. Matter 20 (2008) 365219-1–8.
9. P. Loiko, M. Chen, J. M. Serres, L. Zhang, Z. Lin, H. Lin, G. Zhang, Y. Wang, V. Petrov, U. Griebner, S. Dai, Z. Chen, P. Camy, M. Aguiló, F. Díaz, W. Chen, and X. Mateos, Spectroscopy and high-power laser operation of monoclinic Yb^{3+}:$MgWO_4$ crystal, Opt. Lett. 45 (2020) 1770-1773.
10. L. Zhang, L. Basyrova, P. Loiko, P. Camy, Z. Lin, G. Zhang, S. Slimi, R.M. Solé, X. Mateos, M. Aguiló, F. Díaz, E. Dunina, A. Kornienko, U. Griebner, V. Petrov, L. Wang, W. Chen, Growth, structure and polarized spectroscopy of monoclinic Er^{3+}:$MgWO_4$ crystal, Opt. Mater. Express. 12 (2022) 2028-2040.
11. P. Loiko, J. M. Serres, X. Mateos, M. Aguiló, F. Díaz, L. Z. Zhang, Z. B. Lin, H. F. Lin, G. Zhang, K. Yumashev, V. Petrov, U. Griebner, Y. C. Wang, S. Y. Choi, F. Rotermund, and W. D. Chen, Monoclinic Tm^{3+}:$MgWO_4$: Novel crystal for continuous-wave and passively Q-switched lasers at ~2 μm, Opt. Lett. 42 (2017) 1177-1180.
12. L. Zhang, P. Loiko, J.M. Serres, E. Kifle, H. Lin, G. Zhang, E. Vilejshikova, E. Dunina, A. Kornienko, L. Fomicheva, U. Griebner, V. Petrov, Z. Lin, W. Chen, K. Subbotin, M. Aguiló, F. Díaz, and X. Mateos, Growth, spectroscopy and first laser operation of monoclinic Ho^{3+}:$MgWO_4$ crystal, J. Lumin. 213 (2019) 316-325.
13. P. Loiko, L. Zhang, J.M. Serres, Y. Wang, M. Aguiló, F. Díaz, Z. Lin, H. Lin, G. Zhang, E. Vilejshikova, E. Dunina, A. Kornienko, L. Fomicheva, V. Petrov, U. Griebner, W. Chen, and X. Mateos, Monoclinic Tm:$MgWO_4$ crystal: Crystal-field analysis, tunable and vibronic laser demonstration, J. Alloy Compd 763 (2018) 581-591.
14. L. Zhang, Y. Huang, S. Sun, F. Yuan, Z. Lin, and G. Wang, Thermal and spectral characterization of Cr^{3+}:$MgWO_4$ – a promising tunable laser material, J. Lumin. 169 Part A (2016) 161-164.
15. Y. Wang, W. Chen, M. Mero, L. Zhang, H. Lin, Z. Lin, G. Zhang, F. Rotermund, Y. J. Cho, P. Loiko, X. Mateos, U. Griebner, and V. Petrov, Sub-100 fs Tm:$MgWO_4$ laser at 2017 nm mode-locked by a graphene saturable absorber, Opt. Lett. 42 (2017) 3076-3079.

16. E. Cavalli, A. Belletti, and M. G. Brik, Optical spectra and energy levels of the Cr^{3+} ions in MWO_4 (M = Mg, Zn, Cd) and $MgMoO_4$ crystals, J. Phys. Chem. Solids 69 (2008) 29-34.
17. V.B. Mikhailik, H. Kraus, V. Kapustyanyk, M. Panasyuk, P. Yu, V. Tsybulskyi, L. Vasylechko, Structure, luminescence and scintillation properties of the $MgWO_4$ – $MgMoO_4$ system, J. Phys.: Cond. Matter 20 (2008) 365219-1–8.
18. L. Li, Y. Huang, L. Zhang, Z. Lin, G. Wang, Growth, mechanical, thermal and spectral properties of Cr^{3+}:$MgMoO_4$ crystal, PLoS ONE. 7 (2012) e30327.
19. V. Bakakin, R. Klevtsova, L. Gaponenko, Crystal structure of magnesium molybdate $MgMoO_4$ an example of modified closest packing with two types of tetrahedra, Kristallografiya 27 (1982) 38–42.
20. W. Ran, L. Wang, M. Yang, X. Kong, D. Qu, J. Shi, Enhanced energy transfer from Bi^{3+} to Eu^{3+} ions relying on the criss-cross cluster structure in MgMoO4 phosphor, J. Lumin. 192 (2017) 141–147.
21. L.P. Litovskina, Electron paramagnetic resonance of ions of the 3d and 4f groups in single crystals of $MgMoO_4$, J. Struct. Chem. 7 (1967) 575–577.
22. A.A.G. Santiago, M.C. Oliveira, R.A.P. Ribeiro, R.L. Tranquilin, E. Longo, S.R. de Lázaro, F.V. Motta, M.R.D. Bomio, Atomistic Perspective on the Intrinsic White-Light Photoluminescence of Rare-Earth Free MgMoO4 Nanoparticles, Cryst. Growth Design. 20 (2020) 6592–6603.
23. L.G. Uitert, J.J. Rubin, W.A. Bonner, Preparation of single crystals of tungstates and molybdates of a number of divalent metal ions, J. Am. Ceram. Soc. 46 (1963) 512–512.
24. L.P. Litovskina, M.L. Meil'man, V.G. Andrianov, N.I. Sergeeva, Electron paramagnetic resonance of Cr^{3+} ions in $MgMoO_4$ monocrystals. J. Struct. Chem. 6 (1966) 615–616.
25. D.A. Spasskii, V.N. Kolobanov, V.V. Mikhaĭlin, L.Yu. Berezovskaya, L.I. Ivleva, I.S. Voronina, Luminescence peculiarities and optical properties of $MgMoO_4$ and $MgMoO_4$:Yb crystals. Opt. Spectr. 106 (2009) 556–563.
26. V. Mikhailik, H. Kraus, D. Wahl, M.S. Mykhaylyk, Studies of electronic excitations in $MgMoO_4$, $CaMoO_4$ and $CdMoO_4$ crystals using VUV synchrotron radiation, Phys. Status Solidi B 242 (2005) R17-R19.
27. V.B. Mikhailik, H. Kraus, M. Itoh, D. Iri, M. Uchida, Radiative decay of self-trapped excitons in $CaMoO_4$ and $MgMoO_4$ crystals, J. Phys.: Cond. Matter. 17 (2005) 7209–7218.
28. K.A. Subbotin, Y.S. Didenko, P.A. Popov, A.I. Titov, D.A. Lis, S.K. Pavlov, Y.I. Zimina, K.V. Kuleshova, Growth, thermal conductivity and spectroscopic properties of Nd:$MgMoO_4$ laser crystal, in *International Conference Laser Optics* (IEEE, 2022), P. ThR1-p39, doi: 10.1109/ICLO54117.2022.9840162.
29. G. Han, Z. Xiao-Bin, C. Wen-Ting, Y. Zhi-Feng, P. Jian-Fu, L. Ling-Yun, Y. Yan, Optical spectroscopic properties of Yb^{3+}-doped $MgMoO_4$ crystal grown by the TSSG method, Chinese J. Struct. Chem. 36 (2017) 631–639.
30. M. Morishita, Y. Kinoshita, A. Nozaki, H. Yamamoto, Thermodynamic properties for $MMoO_4$ (M = Mg, Sr and Ba) as the end-members of the yellow phases formed in the nuclear fuel waste glasses, Applied Geochemistry 98 (2018) 310–320.
31. H. Koç, O. Köse, E. Eser, Low-temperature heat capacities for $EMoO_4$ (E=Mg, Sr, Ba) substances formed in nuclear fuel waste glasses, Progr. Nuclear Energy 143 (2022) 104054.
32. M. Gancheva, T. Rojac, R. Iordanova, I. Piroeva, P. Ivanov, Structural and optical properties of $MgMoO_4$ prepared by mechanochemical technique, Ceram. Intern. 48 (2022) 17149–17156.
33. C.S. Xavier, A.P. de Moura, E. Longo, J.A. Varela, M.A. Zaghete, Synthesis and optical property of $MgMoO_4$ crystals, Adv. Mater. Res. 975 (2014) 243–247.
34. L. Zhang, W. He, K. Shen, Y. Liu, S. Guo, Controllable synthesis of hierarchical $MgMoO_4$ nanosheet-arrays and nano-flowers assembled with mesoporous ultrathin nanosheets, Journal of Phys. Chem. Sol. 115 (2018) 215–220.
35. M. Amberg, J.R. Günter, H. Schmalle, G. Blasse, Preparation, crystal structure, and luminescence of magnesium molybdate and tungstate monohydrates, $MgMoO_4 \cdot H_2O$ and $MgWO_4 \cdot H_2O$, J. Sol. State Chem. 77 (1988) 162–169.
36. P. Du, J.S. Yu. Photoluminescence and cathodoluminescence properties of Eu^{3+} ions activated $AMoO_4$ (A = Mg, Ca, Sr, Ba) phosphors, Mater. Res. Bull. 70 (2015) 553–558.
37. L.-Y. Zhou, J.-S. Wei, L.-H. Yi, F.-Z. Gong, J.-L. Huang, W. Wang, A promising red phosphor $MgMoO_4$:Eu^{3+} for white light emitting diodes, Mater. Res. Bull. 44 (2009), 1411–1414.

38. Kim, J. D., & Cho, S. Optical properties of $MgMoO_4$: Dy^{3+}, Eu^{3+} phosphors prepared with different Eu^{3+} molar ratios, J. Korean Inst. Electr. Electron. Mater. Eng. 29 (2016) 186–191.
39. W. Ran, L. Wang, M. Yang, X. Kong, D. Qu, J. Shi, Enhanced energy transfer from Bi^{3+} to Eu^{3+} ions relying on the criss-cross cluster structure in $MgMoO_4$ phosphor, J. Lumin.192 (2017) 141–147.
40. J.E. Miller, N.B. Jackson, L. Evans, A.G. Sault, M.M. Gonzales, The formation of active species for oxidative dehydrogenation of propane on magnesium molybdates, Catal. Lett. 58 (1999) 147–152.
41. L.E. Cadus, M.C. Abello, M.F. Gomez, J.B. Rivarola, Oxidative dehydrogenation of propane over Mg−Mo−O catalysts, Ind. Eng. Chem. Res. 35 (1996) 14–18.
42. P.A. Popov, A.A. Sidorov, E.A. Kul'chenkov, A.M. Anishchenko, I.C. Avetissov, N.I. Sorokin, P.P. Fedorov, Thermal conductivity and expansion of PbF_2 single crystals, Ionics, 23 (2017) 233-239.
43. G.M. Kuz'micheva, V.B. Rybakov, K.A. Subbotin, E.V. Zharikov, D.A. Lis, O. Zaharko, D.A. Nikolaev, V.G. Senin, Russ. J. Inorg. Chem. 57 (2012) 1128.
44. V.F. Tarasov, A.A. Sukhanov, E.V. Zharikov, K.A. Subbotin, D.A. Lis, EPR spectroscopy of impurity ytterbium ions in synthetic forsterite single crystals, Appl. Magn. Res. 53 (2022) 1211–1226.
45. K.A. Subbotin, A.I. Titov, S.K. Pavlov, P.A. Volkov, V.V. Sanina, D.A. Lis, O.N. Lis, Y.I. Zimina, Y.S. Didenko, E.V. Zharikov, Effect of Li^+ codoping on the mechanical strength of Yb:$ZnWO_4$ single crystals, J. Crystal Growth 582 (2022) 126498.
46. A.A. Blistanov, B.I. Galagan, B.I. Denker, L.I. Ivleva, V.V. Osiko, N.M. Polozkov, Yu.E. Sverchkov, Spectral and lasing characteristics of $CaMoO_4$:Nd^{3+} single crystals, Quantum Electron. 19 (1989) 747–748.
47. S.C. Abrahams, Crystal structure of the transition-metal molybdates and tungstates. III. Diamagnetic α-$ZnMoO_4$, J. Chem. Phys. 46 (1967) 2052-2063.
48. M.N. Coelho, P.T.C. Freire, M. Maczka, C. Luz-Lima, G.D. Saraiva, W. Paraguassu, A.G. Souza Filho, P.S. Pizani, High-pressure Raman scattering of $MgMoO_4$, Vibr. Spectr. 68 (2013) 34-39.
49. V.M. Zhukovskii, E.V. Tkachenko, T.A. Rakova, Zhurnal Neorganicheskoj Khimii 15 (1970) 3326-3328.
50. P.A. Popov, S.A. Skrobov, E.V. Zharikov, D.A. Lis, K.A. Subbotin, L.I. Ivleva, V.N. Shlegel', M.B. Kosmyna, A.N. Shekhovtsov, Investigation of the thermal conductivity of tungstate crystals, Crystallogr. Rep. 63 (2018) 111-116.
51. P.J. Miller, The Raman spectra of $MgMoO_4$, Spectrochim. Acta A: Molec. Spectr. 27 (1971) 957-960.
52. Yu.K. Voron'ko, E.V. Zharikov, D.A. Lis, A.V. Popov, V.A. Smirnov, K.A. Subbotin, M.N. Khromov, V.V. Voronov. Growth and spectroscopic studies of $NaLa(MoO_4)_2$:Tm^{3+} crystals: A new promising laser material, Opt. Spectr. 105 (2008) 538–546.